JOURNAL OF MATERIALS SCIENCE 29 (1994) 4314–4318

# Growth of oriented aluminium nitride films on silicon by chemical vapour deposition

A. H. KHAN, M. F. ODEH, J. M. MEESE, E. M. CHARLSON, E. J. CHARLSON, T. STACY, G. POPOVICI*, M. A. PRELAS*, J. L. WRAGG‡
*Electrical and Computer Engineering, *Nuclear Engineering, and ‡Physics and Astronomy, University of Missouri, Columbia, Missouri 65211, USA*

Aluminium nitride films were grown on silicon substrates using the chemical vapour deposition (CVD) method. The properties of the films were studied by scanning electron microscopy (SEM), atomic force microscope (AFM) measurements, X-ray diffraction and Raman scattering. The resulting films were strongly textured and had a preferential orientation with the *c*-axis normal to the surface, the Raman spectra showed two peaks at 607 and 653 $cm^{-1}$ and two large bands at 750 and 900 $cm^{-1}$ of smaller intensity. Both the macro- and micro-Raman spectra showed the same peaks.

## 1. Introduction

Aluminium nitride (AlN) crystallizes in the wurtzite structure with lattice constants $a = 0.311\,14$ nm and $c = 0.497\,92$ nm [1]. AlN is a direct band-gap material with an energy gap of 6.2 eV [2]. It has a high acoustic velocity [3], a high melting point, high electrical resistivity, an excellent thermal conductivity, and high chemical and nuclear stability. With all these properties, AlN has potential use in optical devices operating in the ultraviolet (UV) region, in surface acoustic wave devices, and also as a material for electrically insulating and passivating layers for semiconductors. Progress regarding these applications is slow due to a lack of good single crystals, or at least large-area, highly oriented, dense, defect-free polycrystalline films.

Various techniques, such as reactive sputtering [4], reactive molecular beam epitaxy [5] and chemical vapour deposition (CVD) [2, 6, 7] have been used to grow AlN. CVD is the most widely employed method; it permits the AlN deposition at low substrate temperatures and high deposition rates [2, 8, 9]. It is easy to control while high-purity AlN can be obtained by this method [10].

A variety of substrates, including sapphire [2, 11], α-SiC [12], silicon [6, 9], quartz [13] and others has been used for growth of AlN films. Monocrystalline films have been obtained on basal planes of sapphire [2, 11] and α-SiC [12]. However, these substrates have been used mainly for growth of AlN films for research purposes. Single-crystalline α-SiC is an ideal substrate for the epitaxial growth of AlN films, having the same lattice structure, nearly the same lattice constant (1% mismatch for basal plane), and the same thermal expansion coefficient (TEC) [14]. However, large-area single-crystalline SiC substrates are not available. Sapphire has been used as a substrate to grow AlN films, but the TEC of sapphire is nearly twice that of AlN, therefore usually the films crack on cooling [2].

Silicon substrates have nearly the same TEC as AlN. Silicon is also suitable for industrial applications because of its low cost. Silicon substrates have been used for AlN film growth [6, 9]. Epitaxial AlN has been grown on a limited area of silicon having an orientation relationship of $(0\,0\,0\,1)_{AlN} \| (1\,1\,1)_{Si}$ in the temperature range 1100–1300 °C by the CVD method using $AlCl_3$ and $NH_3$ [6]. However, further study on AlN films grown on silicon substrates at moderate temperature, is required.

In this paper we report the growth of AlN films on silicon substrates at moderate temperatures (700–800 °C) in the pressure range 100–650 torr by the CVD process using $AlCl_3$ and $NH_3$ as the source material. The layers obtained were highly oriented and uniform. The results include scanning electron microscopy, X-ray diffraction and Raman scattering of the film grown. We are reporting, for the first time, AFM measurements and micro-Raman studies on the AlN film grown on silicon substrates.

## 2. Experimental procedure

AlN films were grown on silicon substrates using the CVD method by the chemical reaction of $AlCl_3$ with $NH_3$ in the presence of hydrogen. The overall reaction consists of the formation of a range of aluminium chloride–ammonia complexes, and then the ammonolysis conversion of the complex into AlN and HCl.

A schematic diagram of the CVD apparatus is shown in Fig. 1. The aluminium chloride container was maintained at 150 °C to provide sufficient vapour pressure of aluminium chloride, which was carried into the reaction tube by hydrogen at a flow rate of 120 standard $cm^3\,min^{-1}$. The flow rate of ammonia was 80 standard $cm^3\,min^{-1}$ with 280 standard $cm^3\,min^{-1}$ hydrogen. A part of the reaction tube was maintained at 350 °C by using resistance heating to avoid the condensation of ammonium chloride and aluminium chloride complexes.



0022–2461 © *1994 Chapman & Hall*

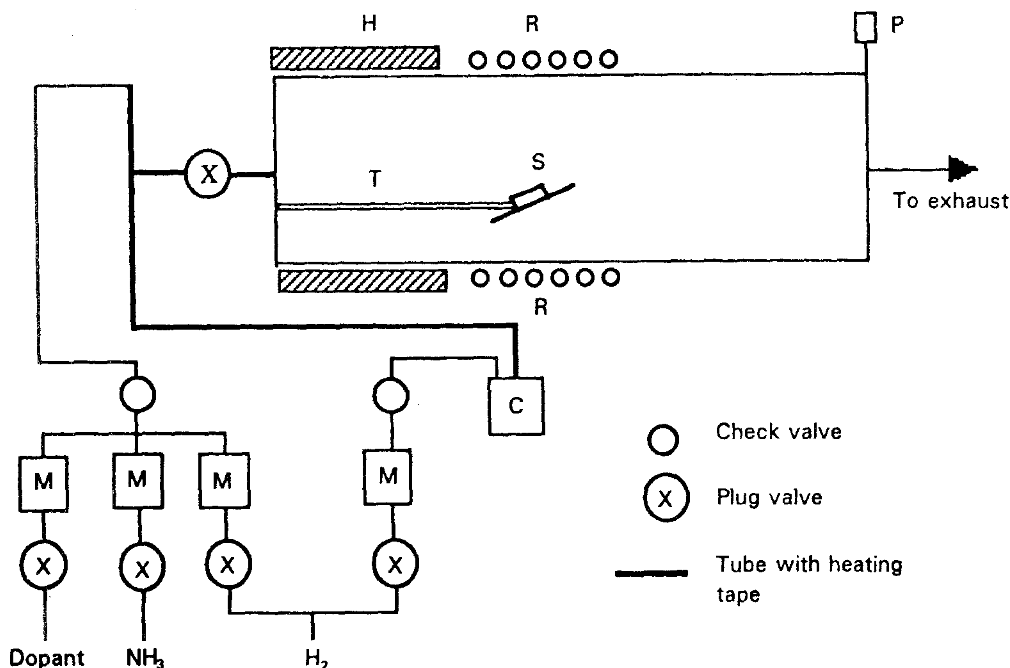


*Figure 1* Schematic diagram of chemical vapour deposition apparatus. C, Aluminium chloride container; H, heating tape; M, mass flow controller; P, pressure transducer; R, r.f. coil; S, susceptor; T, thermocouple.

Prior to growth, the p-type (1 0 0) silicon substrate with 1–3 Ω cm resistivity, was organically cleaned with trichloroethylene, acetone, methanol and de-ionized water in an ultrasonic bath and then briefly annealed in flowing hydrogen near 500 °C prior to growth. About 40 samples at three different experimental conditions were prepared: Type 1 samples of ~ 0.6 μm thickness were grown in 15 min with the reactor chamber pressure of 650 torr and substrate temperature of 700 °C; Type 2 samples of ~ 9 μm thickness were grown in 45 min with a chamber pressure of 200 torr and substrate temperature of 700 °C, and Type 3 samples of ~ 1 μm thickness were grown in 20 min with a chamber pressure of 100 torr and substrate temperature of 800 °C. Both Types 1 and 3 samples were cooled down in 30 min, whereas Type 2 samples were cooled down in 5 min.

The AFM images were recorded in air using the Digital Instruments NanoScope II Atomic Force Microscope.

The Raman spectra were excited by an argon-ion laser operated at 514.5 nm. For the macro-Raman, about 230 mW was incident on the sample. The laser was focused to a spot size of approximately 0.3 $mm^2$ at about 65° from the surface normal. The scattered light was gathered by an off-axis ellipsoid with an $f/1.4$ collection cone centred on the surface normal. For the micro-Raman, about 2 mW was incident on the sample with the laser focused to a spot size of approximately 1 $\mu m^2$. In the spectrograph, a 600 groove/mm grating disperses the signal on to a liquid nitrogen cooled charge coupled device (CCD) detector. The entrance slits were 100 μm wide, corresponding to an instrumental linewidth of about 9 $cm^{-1}$. For the macro-Raman, the signal was integrated for 45 s for the s-polarized and 60 s for p-polarized data. The data were not corrected for detector or grating non-uniformities.

## 3. Results and discussion

All the samples appeared visually under an optical microscope to be smooth and showed good interference fringes on the thin ( ~ 1 μm) films. The scanning electron micrographs of Types 1, 2 and 3 samples are shown in Fig. 2a–c, respectively. Fig. 3 shows the AFM images of all three types of sample. The top view and the surface plot of the same scan area of the Type 1 sample are shown in Fig. 3a and b, respectively. The scanning electron micrograph of Type 1 sample, Fig. 2a, showed a worm-like structure, which actually appeared to be plate-like crystalline structure, as seen by the AFM, Fig. 3a and b. In general, AFM pictures appeared clearer and more suggestive than the scanning electron micrograph.

To determine the roughness of Type 1 sample, the $z$-range was calculated to be 0–75.8 nm with a standard deviation of 9.75 nm. Fig. 3c and d, respectively, show the top view and surface plot of a Type 2 sample. For this sample, the $z$-range was 0–215.47 nm with a standard deviation of 31.43 nm. Fig. 3e and f show the top view and surface plot of a Type 3 sample. This sample had a $z$-range of 0–147.97 nm with a standard deviation of 21.97 nm. For all three types of sample, the grains at the surface have a conical configuration (Fig. 3b, d and f).

Fig. 4 shows the X-ray diffraction patterns for all three types of sample. Types 1 and 2 samples have a preferential orientation with the $c$-axis normal to the surface. However, the degree of orientation is different. The Type 1 sample (Fig. 4a) is strongly oriented giving only the reflection peak (0 0 2) at $2\theta = 36.205°$ (the peak at $2\theta = 69.1°$ is due to the (4 0 0) reflection of the silicon substrate). The full-width at half maximum (FWHM) of the (0 0 2) peak (Fig. 5a) is large ( ~ 1°). The broadening can be due to either the presence of microstresses and/or to the small crystallite size [15].

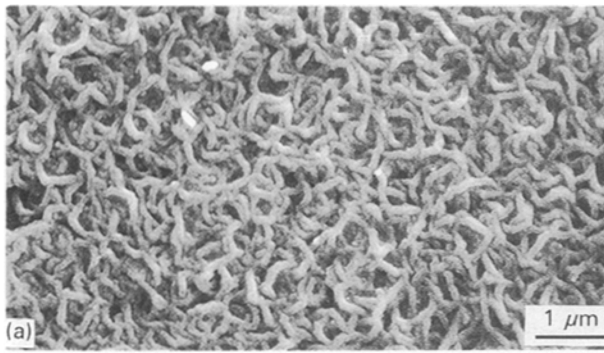


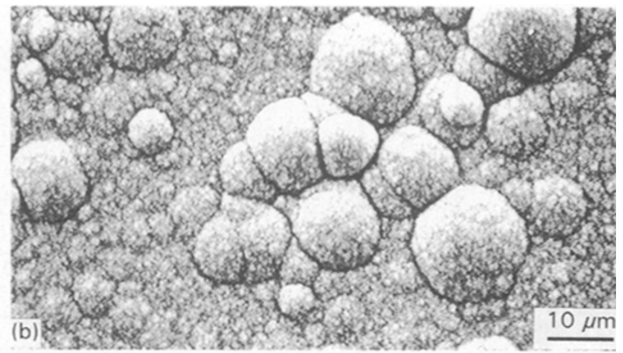


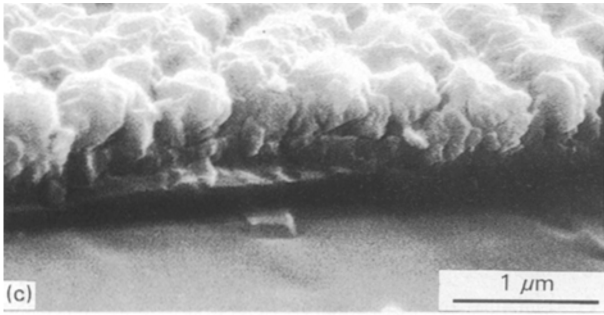


*Figure 2* Scanning electron micrograph of the samples. (a) Type 1, (b) Type 2, (c) Type 3.

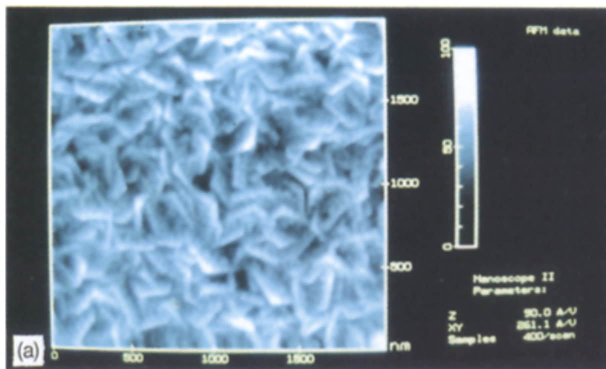


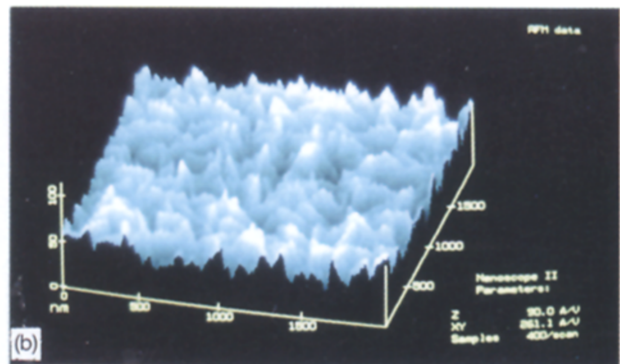


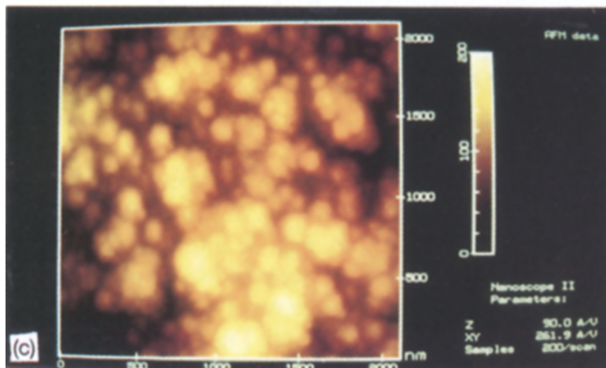


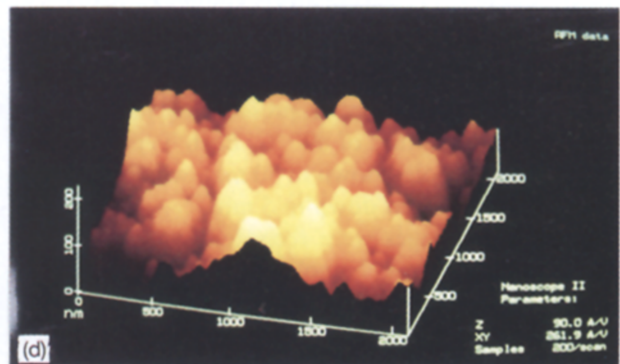


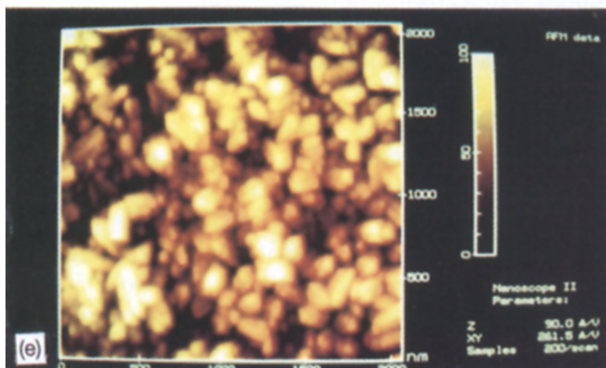


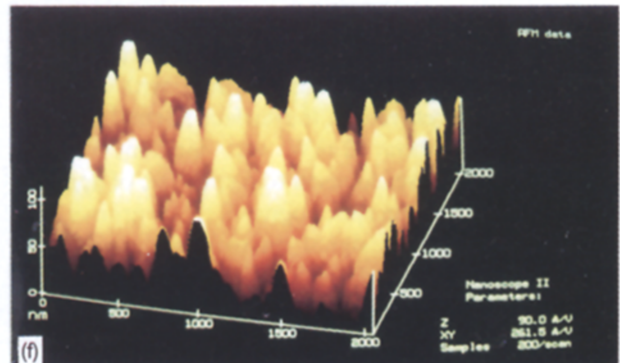


*Figure 3* AFM images. (a) Top view of Type 1, (b) surface plot of Type 1, (c) top view of Type 2, (d) surface plot of Type 2, (e) top view of Type 3, (f) surface plot of Type 3.

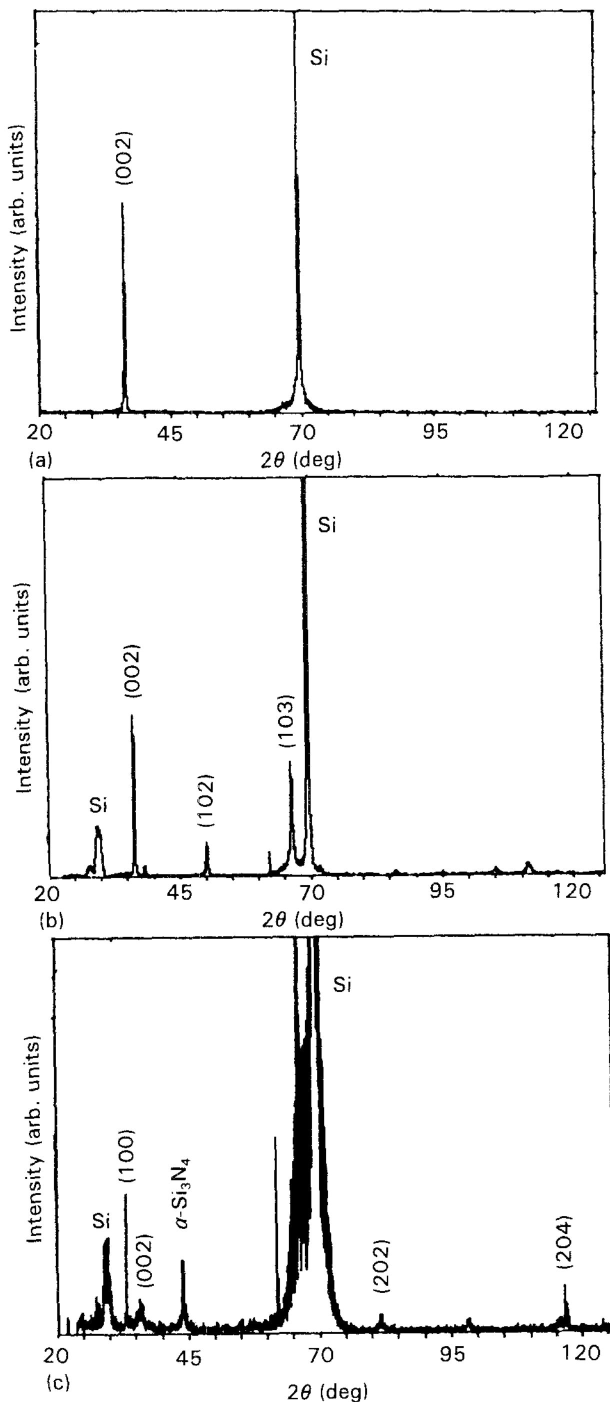


*Figure 4* X-ray diffraction patterns of the samples. (a) Type 1, (b) Type 2, (c) Type 3.

For the (0 0 2) direction the crystallite size is seen along the film depth, so it is expected to be given by the film thickness ( ~ 0.6 μm). This would give no grain-size broadening. Microstresses remain, therefore, the most plausible cause of the observed broadening. The rocking curve for this sample for the (0 0 2) line at fixed detector angle is presented in Fig. 5b. The rocking curve shows that the $c$-axis orientation distribution around the normal to the surface has a FWHM of 15°. The lattice constant determined from the (0 0 2) peak, $c = 0.4958$ nm, is smaller than the ASTM tables value of $c = 0.497\,92$ nm. This shows that the layer is stretched in the basal plane and, therefore, compressed in the $c$-direction provided that the unit volume is approximately the same as in the bulk material.

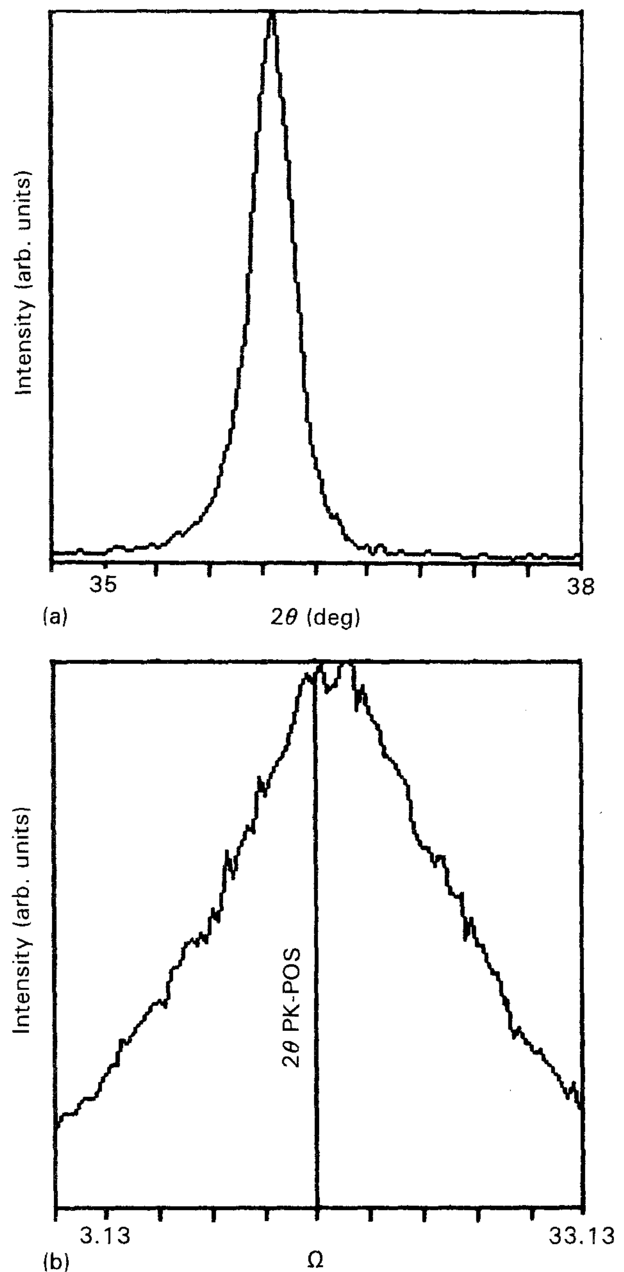


*Figure 5* X-ray rocking curve of Type 2 sample.

The X-ray diffraction pattern for the Type 2 sample (Fig. 4b) has no (1 0 0) reflection. The three strong peaks obtained, (0 0 2) at $2\theta = 36.205°$, (1 0 2) at $2\theta = 49.972°$ and (1 0 3) at $2\theta = 66.955°$ indicate growth with $c$-axis preferentially normal to the surface. The difference between measured and tabulated $d(h\,k\,l)$ values ($d(h\,k\,l)^{M} - d(h\,k\,l)^{ASTM}$) for (0 0 2), (1 0 2) and (1 0 3) are $-0.0011$, $-0.0005$ and $-0.001\,69$ nm, respectively. These differences are caused by stress.

Fig. 4c shows the X-ray diffraction pattern for a Type 3 sample. The 33.037°, 36.096°, 81.529° and 116.612° peaks are for (1 0 0), (0 0 2), (2 0 2) and (2 0 4) AlN. The peak at $2\theta = 43.759°$ is due to (3 0 1) $\alpha$-$Si_3N_4$. Type 3 samples showed (1 0 0) peaks indicating growth with the $c$-axis parallel to the surface.

Macro-Raman spectra of a Type 2 sample are presented in Fig. 6 for s and p polarized light. There is no qualitative difference in the spectra for the two polarizations which would be expected for a polycrystalline sample. The spectra have two peaks at 607

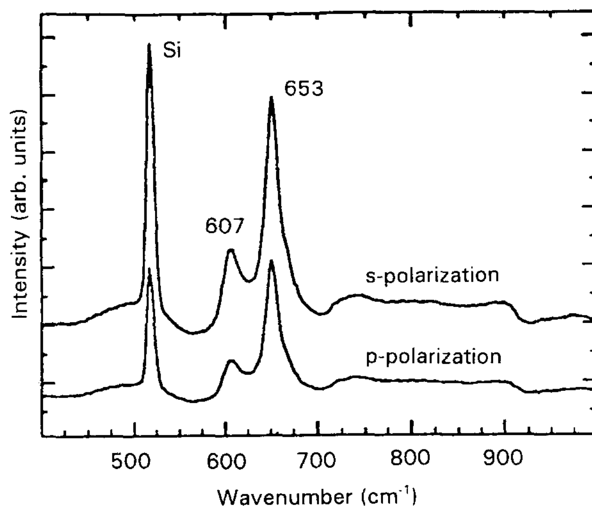


*Figure 6* Macro-Raman spectrum of Type 2 sample.

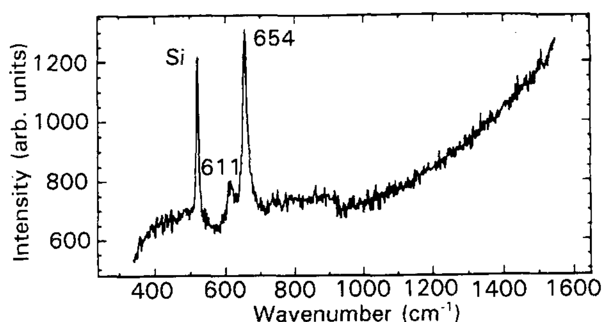


*Figure 7* Micro-Raman spectrum of Type 2 sample.

and 653 $cm^{-1}$, and two large bands around 750 and 900 $cm^{-1}$ of much smaller intensity. The largest peak at 653 $cm^{-1}$ (655 $cm^{-1}$ [16] and 649 $cm^{-1}$ [17]) was attributed to TO phonons, observed also in infrared reflectivity measurements at 666 $cm^{-1}$ [18, 19]. The large weak band at 910 $cm^{-1}$ was observed by Brafman *et al.* [16] and was attributed to LO phonons. It was observed also in infrared reflectivity spectra at 911 $cm^{-1}$ [18] and 902 $cm^{-1}$ [19]. Fig. 7 shows the micro-Raman spectrum of the same sample. The same peaks as in the macro-Raman spectrum are seen. Raman spectra at different points of the sample were recorded for both cases and the same peaks were observed. This confirms good quality and uniformity of the grown films.

## 4. Conclusions

AlN layers were grown on silicon by CVD at moderate temperatures (700–800 °C) using $AlCl_3$ and $NH_3$ as source materials. The AFM measurements showed the films were smooth, and a small value of roughness (between 76 and 215 nm) for different samples was found.

The X-ray diffraction study showed that the layers grown had a preferential orientation with the *c*-axis normal to the surface (Types 1 and 2) and parallel to the surface (Type 3). The $d(h\,k\,l)$ values calculated were smaller than the ASTM values due to the stress in the grown layers.

The Raman spectra showed that the films grown were uniform and of good quality. The spectra had a peak at 653 $cm^{-1}$ due to TO phonons and a large weak band at 910 $cm^{-1}$ due to LO phonons.

## Acknowledgements

The authors thank the Department of Energy, USA, for providing funds for the project, and Mr L. M. Ross and Mr N. Zhao for their assistance in the XRD and SEM studies. J. L. W. thanks the US Army Research Office (Research Triangle Park, NC) for Contract DAAL03-89-K-0084.

## References

1. ASTM card 25-1133 (American Society for Testing and Materials, Philadelphia, PA, 1975).
2. W. M. YIM, E. J. STOFKO, P. J. ZANZUCCHI, J. I. PANKOVE, M. ETTEHBERG and S. L. GILBERT, *J. Appl. Phys.* **44** (1973) 292.
3. M. T. DUFFY, C. C. WANG, G. D. O'CLOCK Jr, S. H. McFARLANE III and P. J. ZANZUCCHI, *J. Electron. Mater.* **2** (1973) 359.
4. A. J. SHUSKUS, T. M. REEDER and E. L. PARADIS, *Appl. Phys. Lett.* **24** (1974) 155.
5. S. YOSHIDA, S. MISAWA, Y. FUJII, S. TAKADA, H. HAYAKAWA, S. GONDA and A. ITOH, *J. Vac. Sci. Technol.* **16** (1979) 990.
6. A. J. NOREIKA and D. W. ING, *J. Appl. Phys.* **39** (1968) 5578.
7. M. MATLOUBIAN and M. GERSHENZON, *J. Electron. Mater.* **14** (1985) 633.
8. J. L. DUPUIE and E. GULARY, *Appl. Phys. Lett.* **59** (1991) 549.
9. M. MORITA, S. ISOGAI, N. SHIMIZU, K. TSUBOUCHI and N. MIKOSHIBA, *Jpn. J Appl. Phys.* **20** (1981) L173.
10. L. M. SHEPPARD, *Ceram. Bull.* **69** (1990) 1801.
11. M. MORITA, N. UESUGI, S. ISOGAI, K. TSUBOUCHI and N. MIKOSHIBA, *Jpn. J. Appl. Phys.* **20** (1981) 17.
12. T. L. CHU, D. W. ING and A. J. NOREIKA, *Solid-State Electron.* **10** (1967) 1023.
13. H. KOMIYAMA and T. OSAWA, *Jpn. J. Appl. Phys.* **24** (1985) L795.
14. Y. S. TOULOUVIAN, R. K. KIBY, R. E. TAYLOR and T. Y. R. LEE, "Thermophysical Properties of Matter", Vol. 13 (IFI/Plenum, New York, Washington, 1977) pp. 154, 873.
15. B. E. WARREN, "X-Ray Diffraction" (Dover, New York, 1990), pp. 298–305.
16. O. BRAFMAN, G. LENGYEL, S. S. MITRA, P. J. GIELISSE, J. N. PLENDL and L. C. MANSUR, *Solid State Commun.* **6** (1968) 523.
17. W. CHANGWEN and L. LING, *J. Non-Cryst. Solids* **112** (1989) 296.
18. A. T. COLLINS, E. C. LINGHUWLERS and P. J. DEAN, *Phys. Rev.* **158** (1967) 833.
19. I. AKASAKI and M. HASHIMOTO, *Solid State Commun.* **5** (1967) 851.

*Received 15 December 1992*
*and accepted 30 April 1993*